PERGAMON

International Journal of Multiphase Flow 28 (2002) 167–174

International Journal of Multiphase Flow

www.elsevier.com/locate/ijmulflow

Brief communication

Mean velocity distributions in a horizontal air–water flow

Somchai Wongwises [a,*], Vladimir Kalinitchenko [b]

[a] *Thermal Engineering and Multiphase Flow Research Laboratory (FUTURE), Department of Mechanical Engineering, Fluid Mechanics, King Mongkut's University of Technology Thonburi, Bangmod, Bangkok 10140, Thailand*

[b] *Institute for Problems in Mechanics, Russian Academy of Sciences, Vernadsky Ave. 101, Moscow 117526, Russia*

Received 18 May 2001; received in revised form 15 August 2001

1. Introduction

Problems involving the interaction between an air stream and a water layer flowing parallel to it or being stagnant are commonly met in engineering and geophysical practice (see Butterworth and Hewitt, 1977; Phillips, 1977). Existing theories are unable to give detailed and quantitative explanations of the mechanism of drift current and wave generation and rely to a large extent on empirical results. Experimental investigations of flow structure therefore play a key role in the development of knowledge in this field. Data in horizontal air–water flow presented here is to gain essential information on current structure inside air and water layers. Velocity measurements of some relevance to this study have been reported in Hanratty and Engen (1957), Lin and Gad-el-Hak (1984), Caulliez (1987), Paras and Karabelas (1992), Paras et al. (1998). The determination of the velocity field has been made either in water (see Baines and Knapp, 1965; Goossens et al., 1982; Kranenburg, 1985; Caulliez, 1987; Tsanis, 1989; Paras and Karabelas, 1992) or in air (see Hanratty and Engen, 1957; Wu, 1975; Lin and Gad-el-Hak, 1984; Paras et al., 1998). In principle, the results so obtained are generally incomplete for lack of simultaneous measurements of air and water velocity profiles under the same experimental conditions. In the present work, we are mainly interested in water and air velocity fields when the interface is undisturbed and transition from stratified to wavy flow takes place. The interaction of two-phase streams is reflected in the form of the velocity profiles.

2. Experimental setup and procedure

The velocity measurements were carried out in an experimental setup developed at FUTURE, where cocurrent horizontal air–water flow was established in a 54×54 mm rectangular channel

* Corresponding author. Tel.: +662-02470-9115; fax: +662-02470-9111.
E-mail address: somchai.won@kmutt.ac.th (S. Wongwises).

0301-9322/02/$ - see front matter
PII: S0301-9322(01)00056-8

with a 2.2 m long straight test section. The setup included the test section, air supply, water supply, instrumentation, and data acquisition system (see Wongwises et al., 1999). Water was pumped from the storage tank through the rotameter to the inlet section at the bottom of the feed pipe. A suction-type blower supplied air to the test section. It passed through a filter and then entered the mixing section through the pressure regulator. Both the air and water streams were brought together in a mixer and then passed through the test section cocurrently. The air velocity could be varied from 0.5 to 10 m/s and the water velocity from 0 to 30 cm/s. Although the water surface elevation along the downwind shore was raised to a sizable amount (~1–2 mm), producing the wind setup, the fetch length which is a length of wind action on the interface, was 10^3 or more times this dimension.

Velocity distributions were measured across the channel at the distance $x = 140$ cm from the inlet. A He–Ne based Laser Doppler Anemometer (LDA-03, Dantec) with photomultiplier was employed in order to make measurements of local horizontal velocity within the liquid phase. The ellipsoidal measuring volume, formed by the intersection of two focused laser beams, had major and minor axes 3.5 and 0.25 mm, respectively. The photomultipliers output signal caused by forward-scattered light was fed to the flow velocity analyzer FVA58N20 which performed statistical analysis of Doppler signal. The traverse mechanism provided precise spatial movement of the measuring volume. For each run, measurements of local instantaneous horizontal velocity, u, were made along the vertical channels direction, y, starting at a distance as close as 0.5 mm from the channel bottom and ending 0.5–1.5 mm from the air–water interface to avoid light reflections.

Air velocity in a cocurrent flow was measured by using constant temperature anemometer (CTA-90CN10/C10, Dantec) with automatic probe setup and execution of experiments. The StreamWare software setup the anemometer modules, performed velocity and directional calibrations and provided an experiment platform, where automatic sequences of hardware setup, data acquisitions and data reductions could be carried out. The probe used in this experiment was the wedge-shaped, right-angled film probe 55R33 with noncylindrical sensor in 1×0.2 mm. The probe was placed on a carrier which could be positioned anywhere in a given section of the channel. The error of the velocity measurements was about 8–10%. The surface velocity of the water was estimated roughly by placing small 2 mm diameter paper pieces on the water and measuring the time required for them to move past fixed stations downstream.

3. Results and discussion

Before the main experiments, the velocity profile in single-phase air–water flow was measured to assess the overall accuracy of experimental results. The mean streamwise velocities measured in the channel for the five different cases are plotted in semi-logarithmic form in Fig. 1. Reynolds numbers of 5535, 15 862, 17 786, and 23 670 described symmetric air flow, and the Reynolds number of 7250 depicted the asymmetric open-channel flow of water with zero shear stress at the free surface. The Reynolds number, Re, is based on the maximal velocity, flow depth and kinematic viscosity: $u_{max} = 1.64$, 4.70, 5.27, and 7.01 m/s, and $h_1 = 54$ mm, $v_1 = 0.12$ cm^2/s for air, and $u_{max} = 1.64$ cm/s, $h_2 = 25$ mm, $v_2 = 0.01$ cm^2/s for water, respectively. The vertical coordinate, y, and the mean velocity, u, were rescaled on the basis of wall-related variables, $u^+ = u/u^*$, $y^+ = yu^*/v$, where u^* is the friction velocity defined by

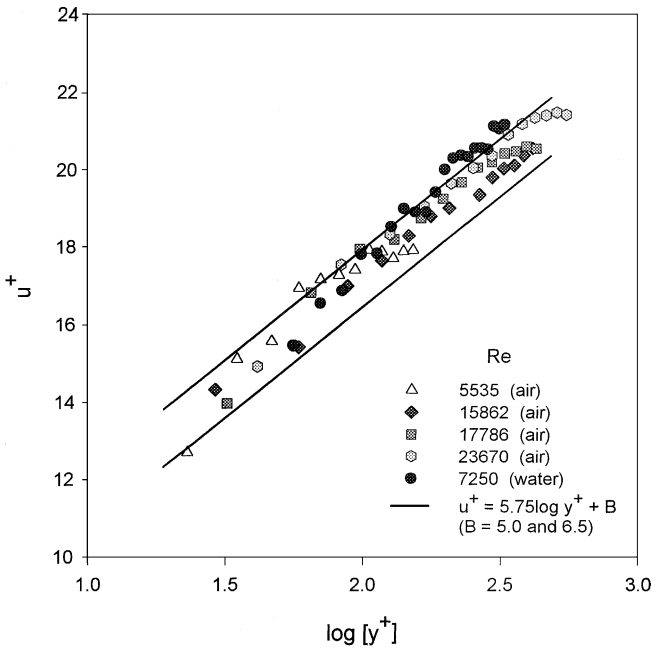

Fig. 1. Velocity distribution on the depth of the single phase flow; air: $Re = 5535$, 15 862, 17 786 and 23 670; water: $Re = 7250$, calculation: $u^+ = 5.75 \log y^+ + B$ ($B = 5.0$ and 6.5).

$$u^* = 0.477 u_{\max} / \ln(0.06 Re_x). \tag{1}$$

The local Reynolds number, Re_x, is defined by $Re_x = u_{\max} x/v$, where v is kinematic viscosity and x is the measuring section of the channel (140 cm). Fig. 1 shows the relationship between $\log y^+$ and u^+ measured with CTA and LDA. The lines represent log-law, $u^+ = 5.75 \log y^+ + B$ (Schlichting, 1951), with $B = 5.0$ and 6.5, respectively. Good agreement between the measured values and those predicted by well-known universal velocity profile was obtained.

The mean streamwise air velocities measured in the channel for the different cases for a stagnant water are plotted in Fig. 2 and those for a flowing water in Fig. 3. The coordinate y in these figures was measured from the undisturbed air–water interface to the top of the channel wall. In all cases, the plane of maximum air velocity was located closer to the air–water interface. In the former case, the plane of maximum velocity was determined by $y/h_1 \approx 0.40$; in the latter case, $y/h_1 \approx 0.45$. Up to maximal air velocity, $u_{\max}$, of about 4.6 m/s, no waves appeared on the water surface. When $u_{\max}$ exceeded 4.6 m/s, the small three-dimensional disturbances had wavelengths of 1–2 cm and amplitudes of 0.1–0.2 mm. For the air velocities in the range of $u_{\max} = 6$–8 m/s, significant two-dimensional waves developed from the initial ripples, and traveled with crests approximately normal to the air direction. Under the action of steady air motion, the waves traveled downstream at an increasing celerity (~30–40 cm/s), while growing both in amplitude and in length. In the measurements section, $x = 140$ cm, typical magnitudes of the observed amplitudes and wavelengths were of order of 0.5–1.0 mm and 2.5 cm, correspondingly. These factors allowed the water surface not to be smooth and the shear stress to be larger at the interface than at the top of an enclosed air space. Similar to Parthasaraty and Muste (1994), we can assume

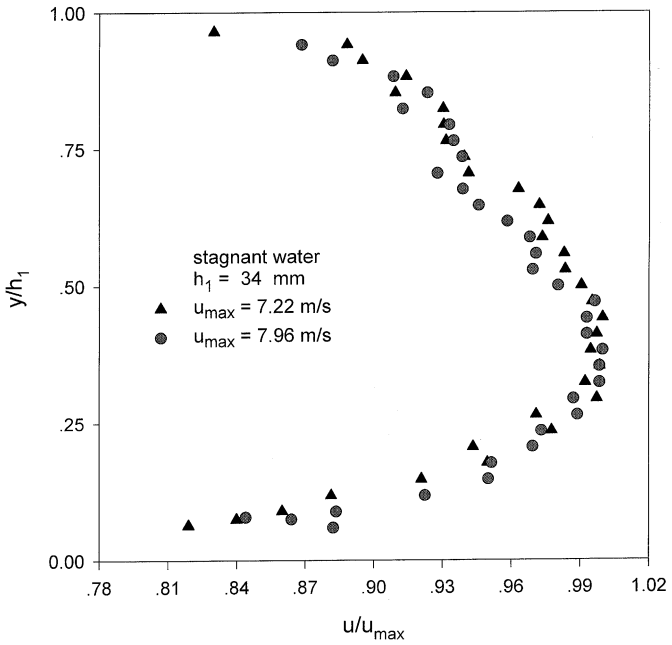

Fig. 2. Typical horizontal air velocity profile along the vertical for a stagnant water. The coordinate y is measured from the undisturbed air–water interface to the top of the channel wall; $h_1 = 34$ mm, $u_{max} = 7.22$ and 7.96 m/s.

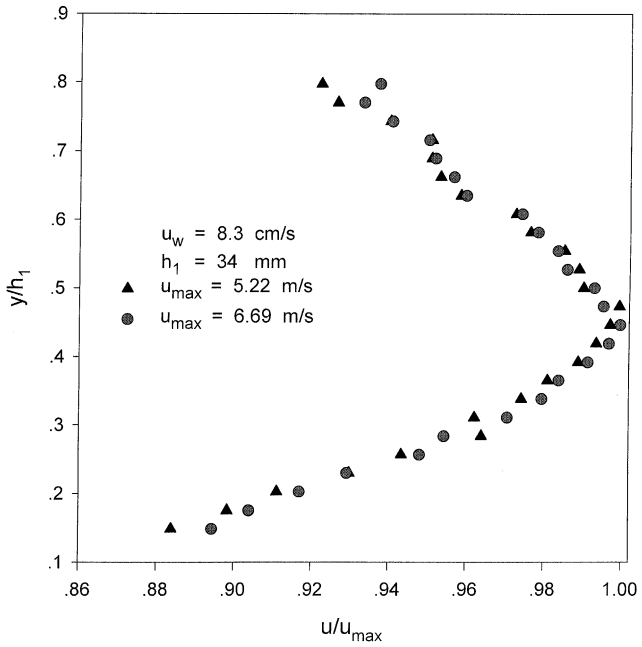

Fig. 3. Typical horizontal air velocity profile along the vertical for a flowing water, $u_w = 8.3$ cm/s. The coordinate y is measured from the undisturbed air–water interface to the top of the channel wall; $h_1 = 34$ mm, $u_{max} = 5.22$ and 6.69 m/s.

the noncoincidence of the plane of maximum air velocity and zero shear stress – it means that the plane of zero shear stress lies closer to the smooth surface, the upper wall. These trends are in agreement with those observed by Paras et al. (1998). However the measured air velocity profiles obtained by Hanratty and Engen (1957) and Dykhno et al. (1994) display a significantly different behavior having their maximal velocity above the center of the air flow space. Their mean shifts are about 10–12% towards the top of the channel wall.

The air flow had a strong influence on the water layer. Since the air was forced by the fan through the channels part of approximately constant cross-section, a pressure gradient was developed in the downstream direction. This pressure gradient increased with air velocity and the water depth. In the closed channel (initially stagnant water) the air flow resulted in a drift current in the upper layer just below the interface and a reverse flow near the bottom. In the case of a flowing water, effect of air was seen in a dramatic distortion of water velocity profiles.

The water surface velocity, u_s, against the maximal air velocity, u_{max}, is shown in Fig. 4. Measurements were conducted in the range of $u_{max} = 3$–8 m/s, thus far, no consideration has been given to the role of breaking waves. The surface velocity ranged from 2 to 18 cm/s and varied nearly quadratically with the air velocity. A curve in Fig. 4 was fitted to the data, with result that $u_s = 0.003\ u_{max}^2$.

Air-driven water currents were investigated in the present experiments for the wide range of maximal air velocity, $u_{max} = 1.0$–8.0 m/s, and two depths of initially stagnant water layer, $h_2 = 12$ and 20 mm. At $u_{max} < 3.5$ m/s, the main water currents followed the air direction, and the return flow near the bottom was small. If u_{max} exceeded 3.5 m/s, a strong return flow was extended to 70% of the water layer except near the surface. Typical distributions of mean water velocity normalized by the surface velocity, u_s, are presented in Fig. 5. Notice that a distinct peak near the

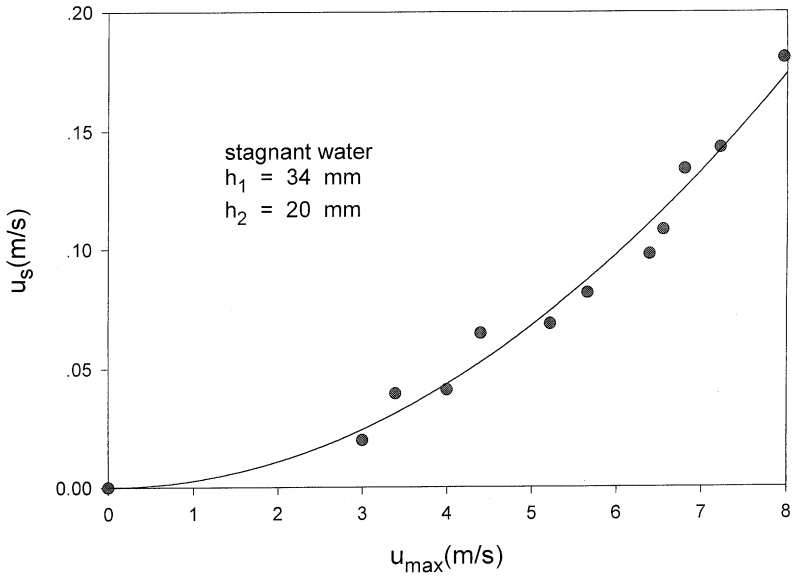

Fig. 4. Water surface velocity, u_s as a function of maximal air velocity, u_{max} (stagnant water, $h_1 = 34$ mm, $h_2 = 20$ mm).

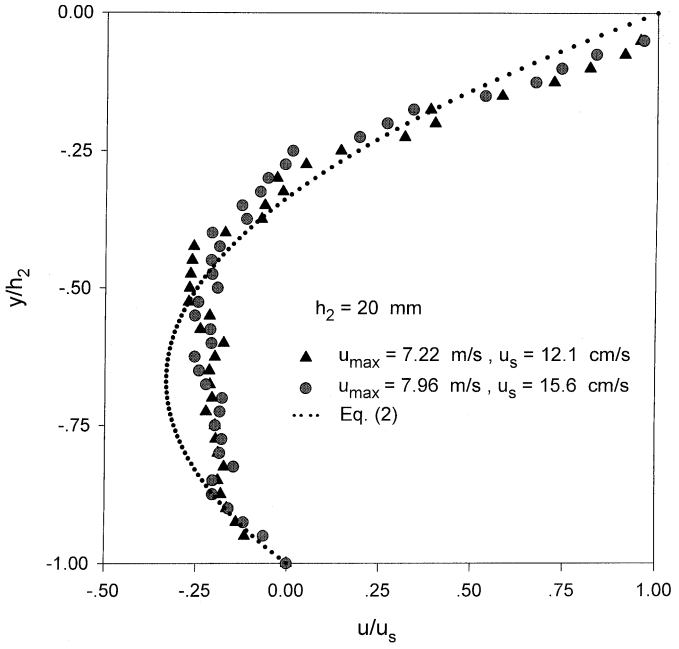

Fig. 5. Distribution of mean velocity in air-driven water currents, $h_2 = 20$ mm: $u_{max} = 7.22$ m/s, $u_s = 12.1$ cm/s and $u_{max} = 7.96$ m/s, $u_s = 15.6$ cm/s.

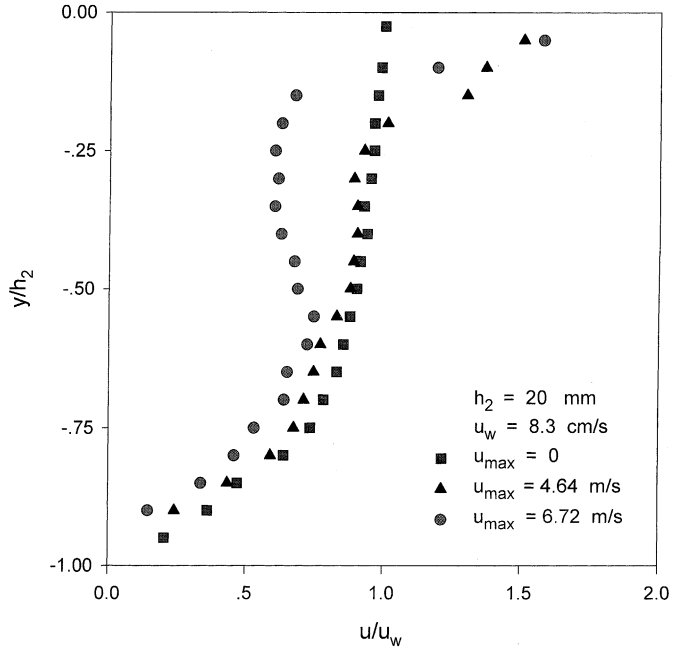

Fig. 6. Distribution of mean velocity in cocurrent air–water flow, $h_2 = 20$ mm, $u_w = 8.3$ cm/s: $u_{max} = 0$, 4.64 and 6.72 m/s.

bottom described by Baines and Knapp (1965) was missed. The curve shown in Fig. 5 corresponds to the well-known parabolic velocity distribution of steady-laminar shear induced flow

$$u/u_s = 1 + 4(y/h_2) + 3(y/h_2)^2. \quad (2)$$

For a cocurrent air–water flow, the distributions of mean water velocity are shown in Fig. 6. The velocity profile for the water flow, $u_w = 8.3$ cm/s, with zero air flow rate was smooth and completely described by the laminar open-channel model. As the air velocity increased and got to $u_{max} = 4.64$ m/s, the jet-like current near the interface was developed. The surface velocity, u_s, was order of 1.5 u_w, and the air-driven current was extended to $0 < y/h_2 < 0.2$. For the air velocity in the range of $u_{max} = 5$–8 m/s, the surface velocity increased, $u_s \approx 2u_w$, the current at all layers followed the air direction, and the typical velocity profile had a distinct local minimum $u/u_w \sim 0.6$ at $y/h_2 \approx 0.25$ and a local maximum $u/u_w \sim 0.75$ at $y/h_2 \approx 0.75$. These features of velocity distributions were common for the present experimental conditions, $u_w = 8$–22 cm/s and $h_2 = 12$–20 mm.

4. Conclusion

This paper presents new experimental data on the simultaneous measurement of the velocity profile in the air and underlying water layer. In conclusion, our results show that the interaction between air and water flows produces the displacement of the maximum air velocity plane toward the interphase. This behavior should be taken into account in phenomenological models trying to reproduce the shear stress distribution. We have found that in cocurrent two-phase flow air effect is seen in a dramatic distortion of water velocity profiles.

Acknowledgements

The present work was supported financially by the Thailand Research Fund (TRF) whose guidance and assistance are gratefully acknowledged.

References

Baines, W.D., Knapp, D.J., 1965. Wind driven water currents. J. Hydraul. Div. ASCE 91, 205–221.

Butterworth, D., Hewitt, G.F., 1977. Two-Phase Flow and Heat Transfer. Oxford University Press, Oxford.

Caulliez, G., 1987. Measuring the wind-induced water surface flow by laser Doppler velocimetry. Exp. Fluids 5, 145–153.

Dykhno, L.A., Williams, L.R., Hanratty, T.J., 1994. Maps of mean gas velocity for stratified flows with and without atomization. Int. J. Multiphase Flow 20, 691–702.

Goossens, L.H.J., van Pagee, H.J.A., Tessel, P., 1982. Vertical turbulent diffusion in air-driven water flows. J. Hydraul. Div. ASCE 108, 995–1009.

Hanratty, T.J., Engen, J.M., 1957. Interaction between a turbulent air stream and a moving water surface. AIChE 3, 299–304.

Kranenburg, C., 1985. Mixed-layer deepening in lakes after wind setup. J. Hydraul. Eng. ASCE 111, 1279–1297.

Lin, J.T., Gad-el-Hak, M., 1984. Turbulent current measurements in a wind-wave tank. J. Geophys. Res. 89, 627–636.
Paras, S.V., Karabelas, A.J., 1992. Measurements of local velocities inside thin liquid films in horizontal two-phase flow. Exp. Fluids 13, 190–198.
Paras, S.V., Vlachos, N.A., Karabelas, A.J., 1998. LDA measurements of local velocities inside the gas phase in horizontal stratified atomization two-phase flow. Int. J. Multiphase Flow 24, 651–661.
Parthasaraty, R.M., Muste, M., 1994. Velocity measurements in asymmetric turbulent channel flows. J. Hydraul. Eng. ASCE 120, 1000–1020.
Phillips, O.M., 1977. The Dynamics of the Upper Ocean. Cambridge University Press, London.
Schlichting, H., 1951. Grenzschicht-Theorie. Braun GmbH, Karlsruhe.
Tsanis, I.K., 1989. Simulation of wind-induced water currents. J. Hydraul. Eng. ASCE 115, 1113–1134.
Wongwises, S., Pornsee, A., Siroratsakul, E., 1999. Gas-wall shear stress distribution in horizontal stratified two-phase flow. Int. Comm. Heat Mass Transfer 26, 849–860.
Wu, J., 1975. Wind-induced drift currents. J. Fluid Mech. 58, 49–70.